# Surface Shear Near the Contact Line of a Binary Evaporating Curved Thin Film

A model for surface shear in the contact line region of a steady state two-component evaporating thin film in the shape of a meniscus is developed. A constant vapor pressure boundary condition at the liquid-vapor interface is combined with experimental meniscus profile data to obtain temperature and composition profiles. The results are used to delineate the relative effects of meniscus shape, temperature, and composition on fluid flow toward the higher temperature in an evaporating meniscus. For the system analyzed, it is found that surface shear due to composition gradients and temperature gradients is the single most important contribution to flow in the evaporating, two-component capillary meniscus in the film thickness range $10^{-6}$ m $\leq \delta \leq 10^{-5}$ m. The effect of concentration on the vapor pressure leads to a maximum evaporation rate at a thickness of approximately 6 $\mu$m for the conditions studied. Theoretical results are discussed in the light of experimental observations.

**C. J. Parks, P. C. Wayner, Jr.**
Department of Chemical Engineering
Rensselaer Polytechnic Institute
Troy, NY 12180

## Introduction

The high heat transfer rates possible in change-of-phase heat transfer have been utilized in capillary devices such as heat pipes, grooved evaporators, sweat coolers, and suction nucleate boilers. In each of these devices the necessary fluid flow in an evaporating thin liquid film is provided by the interfacial free energy. Curvature gradients, surface tension gradients, and gradients in intermolecular forces between the solid and the liquid are all factors in determining the fluid flow rate and, therefore, the heat transfer characteristics. In addition to change-of-phase heat transfer, these phenomena are of fundamental importance in liquid film distillation.

A review of the early literature on evaporative convection in general, with particular emphasis on fluid layers in which the thinness of the layer is important, is given by Berg et al. (1966). Much of the literature on Marangoni phenomena is reviewed by Scriven and Sternling (1960) and by Kenning (1968).

With regard to the specific system of interest herein, numerous experimental investigations have been performed in an attempt to understand more fully evaporation from and fluid flow in a meniscus formed on a flat solid substrate. For example, Renk and Wayner (1979) used interferometry to study a steady state evaporating ethanol meniscus on a horizontal glass plate. They concluded that the evaporating meniscus is stable and that its shape is a function of heat flux. Sharp (1964) and Voutsinos and Judd (1975) used a similar technique to study the transient process of evaporation of the microlayer in nucleate boiling. In a recent set of publications (Cook et al., 1981; Tung, 1982; Tung et al., 1982; Wayner et al., 1983; Tung and Wayner, 1984; Wayner et al., 1985), the use of a scanning microphotometer to help determine the heat transfer characteristics of a thin steady state evaporating liquid film in the thickness range $10^{-7}$ m $< \delta <$ $10^{-5}$ m is described. A simple diagram of the system is shown in Figure 1. A thin silicon wafer was partially submerged in a pool of liquid, forming an extended meniscus. Heat supplied to the upper end of the plate caused fluid to evaporate, resulting in flow from the pool to the meniscus. The microphotometer was used to determine the thickness profile by measuring the relative locations of interference fringes. Since various mechanisms causing fluid flow are functions of the film profile, the profile could be used to evaluate the extent of these mechanisms for various combinations of heat input and fluid system. The initial experiments (Cook et al., 1981) involved relatively pure fluids and were designed to measure the effect of evaporation rate on the meniscus profile. The evaporating thin films were found to be very stable, with fluid flowing toward the heat source. In the subsequent studies it was experimentally demonstrated that small changes in the bulk composition significantly altered the characteristics of the transport processes in the contact line

Correspondence concerning this paper should be addressed to P. C. Wayner, Jr.

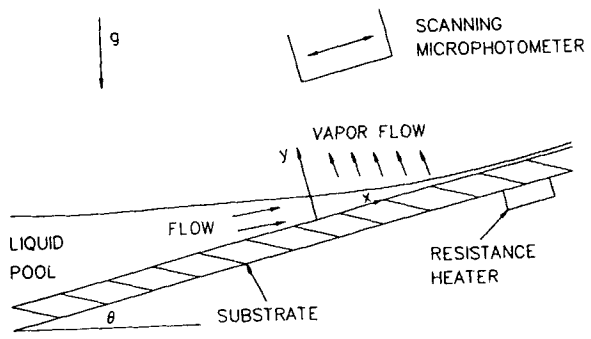


**Figure 1. Evaporating extended meniscus on an inclined flat plate immersed in a pool of liquid.**

region. It became apparent that even small quantities of an impurity with a substantially lower vapor pressure concentrated at the hotter end of the plate as a result of distillation as fluid flowed toward the heat source. The curvature gradient at the liquid-vapor interface was found to be a strong function of heat input and bulk composition, and to be strongly coupled to the concentration gradient. Concentration and temperature gradients apparently caused interfacial shear stresses and fluid flow patterns that enhanced contact line stability. Although the thickness profile could easily be measured optically, the concentration and temperature profiles in a region less than one millimeter in length could not easily be obtained experimentally. Therefore, extensive modeling of the fluid flow mechanisms is needed and is addressed herein.

The experimental results on evaporating thin films of mixtures parallel in many ways the pioneering experimental results obtained by Bascom et al. (1964) on spontaneous spreading with extremely low evaporation rates. Surface tension gradients caused by concentration gradients were identified as the driving force. That work was extended by Ludviksson and Lightfoot (1971), who used a nonisothermal plate with its warm end partially immersed and fluid flowing away from the heat source. More recently, Mirzamoghadam and Catton (1985a) used laser holographic interferometry to study water and Freon-11 on a partially submerged copper plate. They were able to characterize the meniscus in a region where natural convection, conduction, and surface tension gradients due to temperature gradients are important.

Additionally, many theoretical and analytical investigations have been undertaken. Deryagin et al. (1965) conclude that film transport due to intermolecular forces in very thin films is capable of enhancing the evaporation rate from capillaries several times. Potash and Wayner (1972) modeled the transport processes occurring in an evaporating meniscus and adsorbed thin film and concluded that a decrease in thickness of the adsorbed thin film in the contact line region resulting from evaporation can cause fluid flow. Huh and Scriven (1971) discussed fluid flow in an ultrathin film at the contact line. Edwards et al. (1974) developed power law solutions for flow in a capillary meniscus on a finned surface. Wayner et al. (1976) obtained an expression for the local heat transfer coefficient of an evaporating film in terms of the properties of the solid-liquid system. Holm and Goplen (1979) developed a model for describing heat and mass transfer from a surface wetted through capillary grooves. They demonstrate the presence of a high heat transfer rate in the thin film transition region that accounts for 80% of the total heat dissipation. Moosman and Homsy (1980) analyzed the details of the evaporation process in the transition region. Mirzamoghadam and Catton (1985b) derived the meniscus profile for Freon-11 on a partially submerged copper plate using an integral approach for the velocity and temperature profiles. Surface-tension-driven flow caused by temperature gradients was identified as being important, but multicomponent liquids in which concentration gradients may be important were not studied. The details of surface-tension-driven flow caused by gradients in composition as well as in temperature needs further evaluation.

The goals of this work are:

- To develop a model that describes flow in a two-component evaporating meniscus which includes contributions caused by surface shear due to gradients in composition and temperature.
- To combine the model with experimental meniscus profile data in order to calculate the temperature and composition profiles as well as the evaporative heat flux distribution in a realistic meniscus.
- To substitute the calculated concentration and temperature profiles back into the equation for flow in order to evaluate the relative importance of the various mechanisms contributing to flow in that portion of the meniscus under investigation and to thereby increase our understanding of the transport phenomena.

Herein, a simple model based on continuum mechanics, interfacial phenomena, one-dimensional heat conduction, a constant vapor pressure boundary condition, and Raoult's law is developed and used to describe fluid flow and heat transfer in an evaporating, two-component meniscus formed on a thin, inclined, heated substrate. The constant vapor pressure boundary condition provides a simple method for analyzing the transport processes in an evaporating meniscus and allows the significance of the various terms contributing to flow to be determined.

For the isothermal case analyzed, the resulting ODE accurately predicts the experimentally observed meniscus profile in the thickness range $10^{-7}\ \text{m} < \delta < 10^{-5}\ \text{m}$. For the nonisothermal case analyzed, a set of six first-order, nonlinear, coupled ordinary differential equations is obtained. When combined with a polynomial representation of experimental meniscus profile data, these equations are solved for the temperature, composition, and mass flow rate in the meniscus as well as the evaporative heat flux. The temperature profiles obtained agree with experimentally observed trends. A maximum evaporation rate is obtained at a thickness of approximately six microns ($\mu$m) for a mixture of 98% decane/2% tetradecane. Since the effects of concentration and adsorption on the vapor pressure can be greater than the effect of a decrease in film thickness on conductance across the liquid film, the evaporative heat flux tends toward zero as the film thickness decreases from the value at the maximum evaporation rate.

The results for temperature and composition, and the polynomial representation of the meniscus profile are substituted back into the model equations and the significance of each mechanism is determined. Flow resulting from surface shear and flow resulting from gradients in curvature are found to be most significant over the thickness range studied and are on the order of 100 times (surface shear) and 10 times (curvature) more important than the gravitational contribution. Surface shear resulting from concentration gradients caused by distillation is found to be greater than and opposed to the surface shear

caused by a temperature gradient alone. The overall effect of surface shear is a net flow toward the heat source, but it should be noted that this is a result of the temperature and composition range in question.

## The Model

A continuum model is used to discuss the physicochemical phenomena of importance to fluid flow in the two-component steady state evaporating meniscus shown in Figure 1.

Neglecting inertia terms and the $y$ component of velocity, the Navier-Stokes equation for velocity in the $x$ direction becomes

$$\mu \frac{\partial^2 u}{\partial y^2} = \frac{\partial}{\partial x}(p_\ell + \phi + \rho g x \sin\theta) = \frac{\partial P}{\partial x} \tag{1}$$

in which

$$p_\ell = p_v - \sigma K + \rho g(\delta - y)\cos\theta \tag{2}$$

and

$$\phi = \frac{-B}{\delta^n} + \phi_B \tag{3}$$

The Young-Laplace equation of capillarity, Eq. 2, is used to model the decrease in pressure on passing from the vapor to the liquid, caused by the curved interface. A potential energy function per unit volume, Eq. 3, is used to model the difference in behavior of a thin film of liquid between two bulk phases relative to the same liquid as a bulk phase (Frenkel, 1955; Dzyaloshinskii et al., 1961; Miller and Ruckenstein, 1974; Ruckenstein and Jain, 1974; Wayner, 1980; Chen and Slattery, 1982). This approach is equivalent to using the disjoining pressure concept (Deryagin et al., 1965; Wayner et al., 1976) but circumvents the need to discuss disjoining pressure explicitly. In either case the results are the same. For films thicker than approximately 400 Å (40 nm) the potential function is inversely proportional to the fourth power of film thickness (Dzyaloshinskii et al., 1961; Churaev, 1974a)

$$\frac{B}{\delta^n} = \frac{\bar{B}}{\delta^4}, \quad \delta > 400 \text{ Å} \tag{4}$$

The constant $\bar{B}$ is a function of the static dielectric constants of the three phases in question (Churaev, 1974a, 1975). For films thinner than approximately 200 Å (20 nm) the potential function is inversely proportional to the thickness cubed (Dzyaloshinskii et al., 1961; Churaev, 1974b).

$$\frac{B}{\delta^n} = \frac{-A_{s\ell v}}{6\pi\delta^3} = \frac{\bar{A}}{\delta^3}, \quad \delta < 200 \text{ Å} \tag{5}$$

In this equation, the Hamaker constant for a spreading system is $A_{s\ell v} < 0$. Wayner (1978) has outlined the procedure for calculating $\bar{A}$ from the macroscopic optical and thermophysical properties of a given system.

Equation 1 is solved using the following boundary conditions

$$y = 0, \quad u = 0 \tag{6}$$

$$y = \delta(x), \quad \tau_{yx} = \mu \frac{\partial u}{\partial y} = \frac{d\sigma}{dx} \tag{7}$$

The boundary condition in Eq. 7 equates the surface shear at the liquid-vapor interface to the surface tension gradient. This boundary condition can have a large effect on the velocity profile because large gradients in concentration and temperature resulting in large surface tension gradients are possible in evaporating thin films. Even a relatively pure bulk fluid can develop large concentration gradients caused by preferential evaporation of the more volatile component. The resulting mass flow rate as given by Wayner and Parks (1985) is

$$\Gamma = \frac{\delta^3}{3\nu}\left[\left(\frac{1.5}{\delta} + K\right)\sigma' + \sigma K' - \frac{nB\delta'}{\delta^{n+1}} + \frac{B'}{\delta^n} - \rho g\delta'\cos\theta - \rho g\sin\theta\right] \tag{8}$$

The prime denotes differentiation with respect to $x$. It has been shown (Wayner and Parks, 1985) that the term $B'/\delta^n$ is insignificant in the region of interest compared to the term $1.5\sigma'/\delta$ and therefore it will be neglected here. Equation 8 is nondimensionalized by dividing both sides of the equation by the flow rate of a uniform liquid film flowing over a vertical flat plate, Eq. 9:

$$\Gamma_{vp} = \frac{\rho g\delta^3}{3\nu} \tag{9}$$

The resulting dimensionless equation is

$$\frac{3\nu\Gamma}{\rho g\delta^3} = \underbrace{\frac{1.5\sigma'}{\rho g\delta}}_{\text{I}} + \underbrace{\frac{K\sigma'}{\rho g}}_{\text{II}} + \underbrace{\frac{\sigma K'}{\rho g}}_{\text{III}} - \underbrace{\frac{nB\delta'}{\rho g\delta^{n+1}}}_{\text{IV}} - \underbrace{\delta'\cos\theta}_{\text{V}} - \underbrace{\sin\theta}_{\text{VI}} \tag{10}$$

Terms III through VI depend primarily on the film profile and can be evaluated from experimental data. The evaluation of terms I and II, which account for flow caused by a surface tension gradient due to gradients in temperature and composition, is the focus of this paper.

For a binary mixture of low molecular weight $n$-alkanes, the surface tension can be adequately represented by (Reid et al., 1977)

$$\sigma = x_1\sigma_1(T_i) + (1 - x_1)\sigma_2(T_i) \tag{11}$$

By the chain rule the following equation for the surface tension gradient is obtained.

$$\frac{d\sigma}{dx} = \left[x_1\frac{d\sigma_1}{dT} + (1 - x_1)\frac{d\sigma_2}{dT}\right]\frac{dT_i}{dx} + (\sigma_1 - \sigma_2)\frac{dx_1}{dx} \tag{12}$$

The surface tensions of the pure components are assumed to be

linear functions of temperature:

$$\sigma_i = a_i + b_i T \tag{13}$$

where the constants $a_i$ and $b_i$ are given by Jasper (1972).

The concentration gradient can be related to the temperature gradient at the liquid-vapor interface through the use of a constant vapor pressure boundary condition (Parks and Wayner, 1985). Physically it seems reasonable to assume that the vapor pressure for a short distance along the vapor-liquid interface is constant and approximately equal to the equilibrium vapor pressure if the interfacial resistance to evaporation is small and if tangential vapor flow occurs rapidly. The vapor pressure of component $i$ in the liquid film is obtained by using Raoult's law.

$$P_{v_i} = x_i P_{v_i}^{sat}(T) \tag{14}$$

The vapor pressures of pure components are calculated from the Antoine equation,

$$\ln P_{v_i}^{sat} = A_i + \frac{B_i}{T + C_i} \tag{15}$$

where the constants are given by Reid et al. (1977). In Eq. 14 the effects of curvature and of interfacial forces on the vapor pressure have been neglected. This model applies to that portion of the meniscus where the curvature is sufficiently small and the thickness sufficiently large that these effects are negligible. The vapor pressure of the film is the sum of the individual vapor pressures of the two components.

$$P_v = P_{v_1} + P_{v_2} = x_1 P_{v_1}^{sat}(T_i) + (1 - x_1) P_{v2}^{sat}(T_i) \tag{16}$$

Differentiating Eq. 16 with respect to $x$ and setting the result equal to zero yields the following equation.

$$\left(1 - \frac{P_{v_2}^{sat}}{P_{v_1}^{sat}}\right)\frac{dx_1}{dx} + \left[x_1 \frac{d \ln P_{v_1}^{sat}}{dT} + (1 - x_1)\frac{P_{v_2}^{sat}}{P_{v_1}^{sat}} \frac{d \ln P_{v_2}^{sat}}{dT}\right]\frac{dT_i}{dx} = 0 \tag{17}$$

Equations 12 and 17 are combined to give the surface tension gradient in terms of the temperature gradient alone. The effects of concentration and temperature on surface shear for the decane(1)/tetradecane(2) system are summarized in Figure 2. The constant vapor pressure condition corresponds to the dashed lines in the figure. For a given temperature on the liquid-vapor interface and a known vapor pressure, the concentration and the surface tension gradient are determined.

The temperature and temperature gradient at the liquid-vapor interface are obtained by assuming one-dimensional heat conduction in the solid in the $x$ direction (experimentally, a thin, high-conductivity substrate was used), and one-dimensional heat conduction in the liquid in the $y$ direction (a thin film with a small velocity was used experimentally). Under these assumptions the temperature at the liquid-vapor interface is given by the following equation.

$$T_i = T_w - \frac{\dot{q}''\delta}{k_\ell} \tag{18}$$

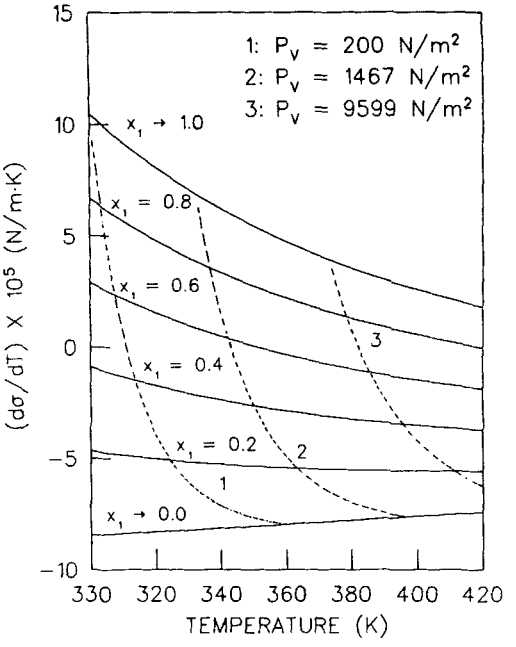


**Figure 2. Surface tension derivative vs. temperature as a function of composition for decane(1)/tetradecane(2) system.**

Differentiating Eq. 18 gives an expression for the temperature gradient at the vapor-liquid interface.

$$\frac{dT_i}{dx} = \frac{dT_w}{dx} - \frac{1}{k_\ell}\left(\dot{q}''\frac{d\delta}{dx} + \delta\frac{d\dot{q}''}{dx}\right) \tag{19}$$

The evaporative heat flux is related to the wall temperature under the one-dimensional heat conduction assumptions by the following equation.

$$\dot{q}'' = -h_{fg}\frac{d\Gamma}{dx} = k_s a \frac{d^2 T_w}{dx^2} \tag{20}$$

It should be noted that this model assumes that the concentration is uniform across the film at any $x$ location and therefore diffusion in the $y$ direction has not been included. Because of concentration gradients in the $x$ direction, there will be diffusion in the $x$ direction; this effect is secondary to the bulk convection term and has been neglected.

## Results and Discussion

### *Equilibrium profile*

At equilibrium (isothermal) conditions the mass flow rate given by Eq. 8 is equal to zero. The temperature gradient is zero, and so by Eq. 17 the concentration gradient is zero. Therefore, by Eq. 12 the surface tension gradient is zero. Using these results in Eq. 8 gives an equation governing the equilibrium profile.

$$\sigma K' - \frac{nB}{\delta^{n+1}}\delta' - \rho g \delta' \cos\theta - \rho g \sin\theta = 0 \tag{21}$$

where the curvature, $K$, is given by

$$K = \frac{\delta''}{(1 + (\delta')^2)^{3/2}} \tag{22}$$

Combining Eqs. 21 and 22 gives a third-order, nonlinear, ordinary differential equation for the film thickness. This can be treated as an initial-value problem by specifying the slope and curvature of the liquid-vapor interface at a given film thickness. This was done for the decane/2% tetradecane system using an implicit integration scheme developed by Hindmarsh (1974) based on the work of Gear (1971). The results are shown in Figures 3 and 4 and are in good agreement with experimental data (Tung, 1982). Figure 4 shows a sharp decrease in curvature near the contact line. This effect is offset by the contribution of the potential function, which becomes large at small thicknesses, resulting in zero net flow. Two regions can thus be defined using the results presented in Figure 4. At thicknesses greater than approximately 1 $\mu$m the meniscus profile is controlled by capillarity, and at thicknesses much smaller than 1 $\mu$m the profile is controlled by the thin film effects of Eq. 3. There is a sharp transition zone between the two regions. Renk et al. (1978) present an "exact" solution to this problem for a slightly different geometry which shows the features of the transition zone between the capillary meniscus and adsorbed thin film using the method of matched asymptotic expansions. Moosman and Homsy (1980) analyzed the transition region for the evaporating case. The length of the transition zone is on the same scale as found in that work.

### *Evaporating meniscus*

For the case of the evaporating meniscus, the experimental profile data of Tung (1982) are combined with the model outlined above to compute the temperature and composition profiles in the meniscus as well as the evaporative heat flux and mass flow rate as functions of thickness. The experimental profile data are fitted to various polynomials of order $m$ in a least-

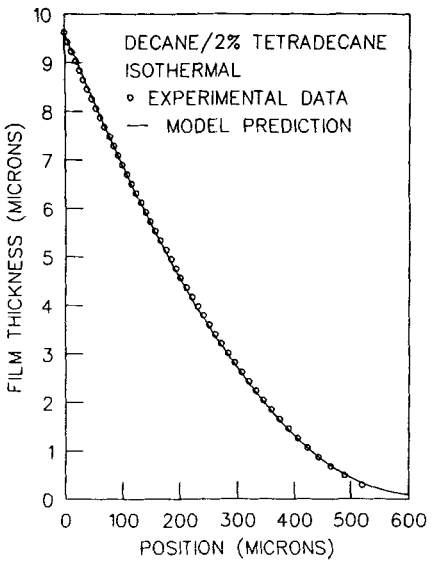


**Figure 3. Thickness vs. position for isothermal case.**

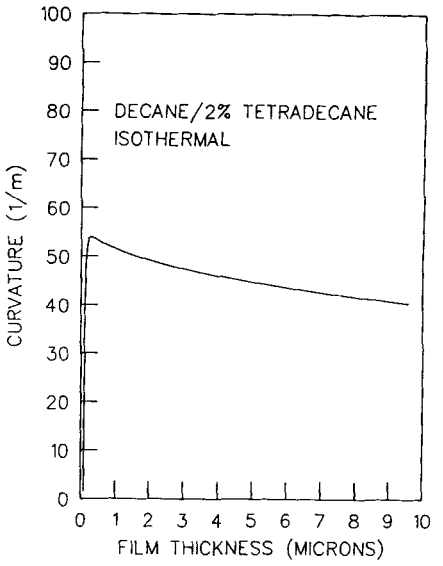


**Figure 4. Curvature vs. thickness based on model for isothermal case.**

squares sense. The polynomial that best represents the data is used in the model. It should be noted that a polynomial fit to the isothermal data shown in Figure 3 cannot generate the curvature profile shown in Figure 4 for the region $\delta < 10^{-6}$ m. The analysis of the nonisothermal case that depends on the polynomial fit is therefore restricted to thicknesses greater than 1 $\mu$m, below which the thin film effects begin to become important. The analysis is still limited in the sense that the meniscus profile is determined *a priori* and in that the solution depends greatly on the choice of polynomial for the experimental data. The results are nevertheless useful in determining the relative importance of the various phenomena contributing to flow in the meniscus.

Equations 8, 12, 17, 19, and 20 form a set of six nonlinear, coupled, first-order ordinary differential equations. The system was treated as an initial value problem by specifying $\Gamma$, $\dot{q}''$, $T_i$, $x_1$, and $dT_w/dx$ at a position corresponding to a film thickness of 9.6 $\mu$m. The system was solved using the same integration scheme employed for the isothermal case.

Two nonisothermal experimental profiles were used with the model. The initial conditions used in the two cases were based in part on experimental observations and are given in Table 1. Experimentally (Tung, 1982; Tung et al., 1982), it was found that the temperature data could be represented well by two straight lines intersecting at a location that corresponded to the contact line region. From the slopes of these straight lines a value of $P_T$, the integral heat sink of the meniscus, is calculated by taking the difference between the heat conducted into and out of the contact line region. The initial flow rate is then calculated by dividing $P_T$ by the latent heat of vaporization.

$$\Gamma_o = \frac{P_T}{h_{fg}} = \frac{k_s a}{h_{fg}} \left( \left. \frac{dT_w}{dx} \right|_f - \left. \frac{dT_w}{dx} \right|_o \right) \tag{23}$$

The initial composition is taken to be that of the bulk (i.e., it is assumed that no distillation takes place between the pool and a film thickness of 9.6 $\mu$m). Iterations are required to find an ini-

**Table 1. Initial Conditions Used in Model**

| | | |
|---|---|---|
| $\delta_o$, m | $9.6 \times 10^{-6}$ | $9.6 \times 10^{-6}$ |
| $P_T$, W/m | 4.9 | 10.0 |
| $\Gamma_o$, kg/m · s | $1.43 \times 10^{-5}$ | $2.93 \times 10^{-5}$ |
| $\dot{q}''_o$, W/m$^2$ | $2.10 \times 10^4$ | $5.10 \times 10^4$ |
| $T_{i_o}$, K | 315 | 332 |
| $m_{1_o}$ | 0.98 | 0.98 |
| $(dT_w/dx)_o$, K/m | 220 | 452 |

**Table 2. Physical Properties Used in Model**

$h_{fg}$ decane ($T$ = 315 K) = 348.9 kJ/kg
$h_{fg}$ decane ($T$ = 332 K) = 341.1 kJ/kg
$h_{fg}$ tetradecane ($T$ = 315 K) = 353.2 kJ/kg
$h_{fg}$ tetradecane ($T$ = 332 K) = 347.1 kJ/kg

$k_\ell = 0.134$ W/m · K
$k_s = 120$ W/m · K
$\bar{A} = 1 \times 10^{-20}$ J; $n = 3$
$\bar{B} = 101.6 \times 10^{-30}$ J · m; $n = 4$

$\nu = 1.25 \times 10^{-6}$ m$^2$s
$\rho = 726.1$ kg/m$^3$
$\sigma_1 = (50.79 - 0.09197\ T/\text{K}) \times 10^{-3}$ N/m
$\sigma_2 = (52.01 - 0.08682\ T/\text{K}) \times 10^{-3}$ N/m

$$\ln\left[P_{v_1}^{sat}/(\text{N/m}^2)\right] = 20.9042 - \frac{3{,}456.8}{T/\text{K} - 78.67}$$

$$\ln\left[P_{v_2}^{sat}/(\text{N/m}^2)\right] = 21.0408 - \frac{4{,}008.52}{T/\text{K} - 105.4}$$

$\theta = 5.8796°$
$a = 3.55 \times 10^{-4}$ m

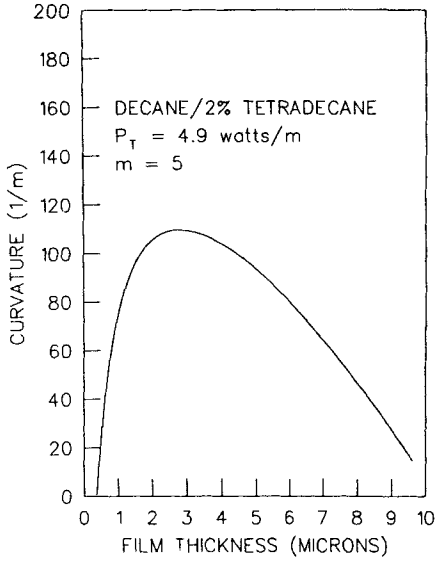


**Figure 6. Curvature vs. thickness for $P_T$ = 4.9 W/m based on polynomial fit of Figure 5.**

tial value of heat flux that produces essentially no flow for a film thickness of 1 $\mu$m. Therefore, the initial heat flux and thereby the heat flux distribution are adjusted until essentially all the fluid evaporates in the region $10^{-6} < \delta < 9.6 \times 10^{-6}$ m. The physical properties used are those of decane evaluated at the initial temperature, except for the surface tension and the vapor pressure, which are treated as functions of both temperature and composition. The physical properties are summarized in Table 2.

Figures 5 and 7 show the experimental profile data as well as the polynomial fit to the data. Figures 6 and 8 show the curvature, calculated from the polynomial, as a function of film thickness. Note that where the curvature gradient is opposed to the direction of flow (i.e., near the contact line) an additional mech-

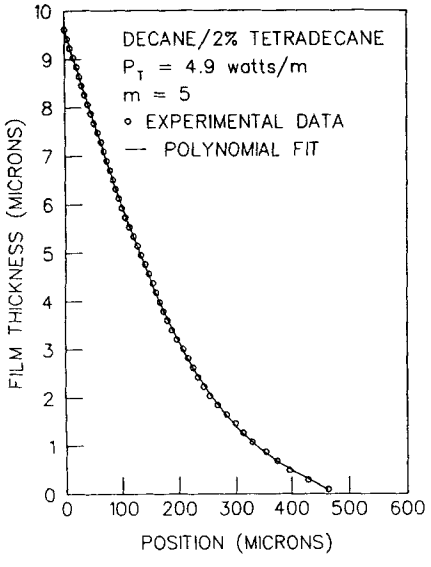


**Figure 5. Thickness vs. position for $P_T$ = 4.9 W/m.**

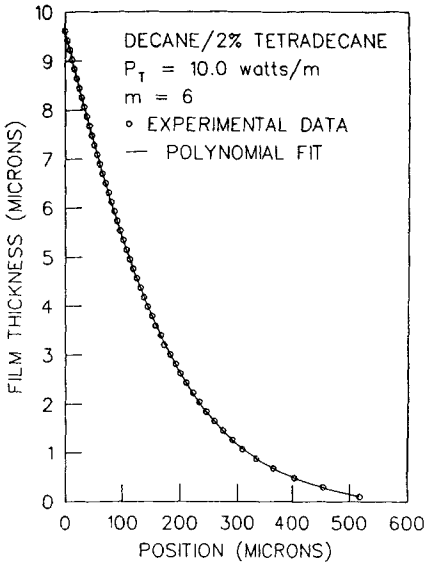


**Figure 7. Thickness vs. position for $P_T$ = 10.0 W/m.**

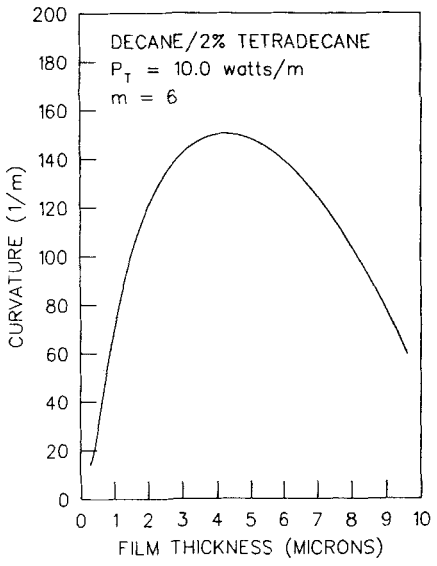


**Figure 8. Curvature vs. thickness for $P_T$ = 10.0 W/m based on polynomial fit of Figure 7.**

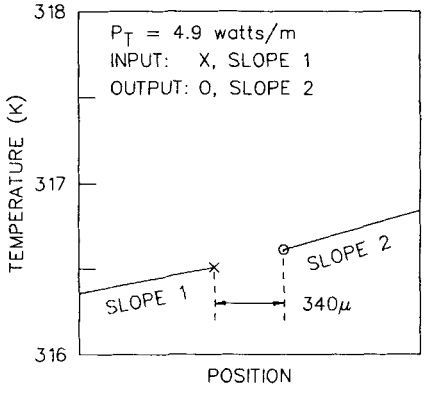


**Figure 9. Comparison of experimental and model temperature profiles for $P_T$ = 4.9 W/m.**

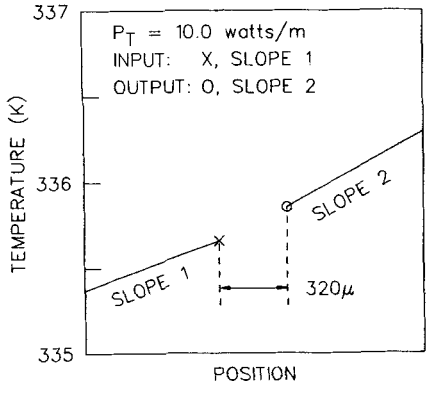


**Figure 10. Comparison of experimental and model temperature profiles for $P_T$ = 10.0 W/m.**

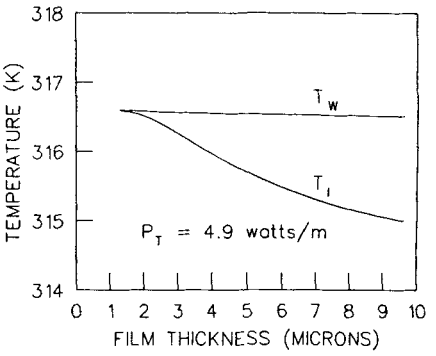


**Figure 11. Predicted wall and interfacial temperature vs. film thickness for $P_T$ = 4.9 W/m.**

anism, acting in the direction of flow, must be present for a stationary meniscus to exist.

Figures 9 through 18 show the numerical results for the two cases studied. Figures 9 and 10 compare the wall temperatures predicted by the model with those obtained experimentally; the temperatures are superimposed. Although temperatures over a distance less than 1 mm could not be measured accurately, the thermocouples gave good estimates of the wall temperature derivative above and below the region where evaporation occurred. This gives a value of $dT_w/dx$ and an approximate value of $T_w$ to be used at a thickness of 9.6 $\mu$m. The model predicted values at a thickness of 1 $\mu$m that are in excellent agreement with the experimentally observed values. Figures 11 and 12 show the details of the temperature profiles for both the wall and the interface for the two cases studied. Figure 13 shows the composition profiles. The direct relationship between interfacial temperature and mole fraction through the constant vapor pressure boundary condition can be seen in the slopes of the curves. As the temperature rises and the vapor pressure of the pure components increases, the mole fraction of component 1 (the component with the higher vapor pressure) decreases, leaving the total vapor pressure unchanged.

The heat flux profiles for the two cases are given in Figure 14. The heat flux is directly related to the second derivative of the wall temperature by Eq. 20. It is also directly related to the difference between the wall and interfacial temperatures divided

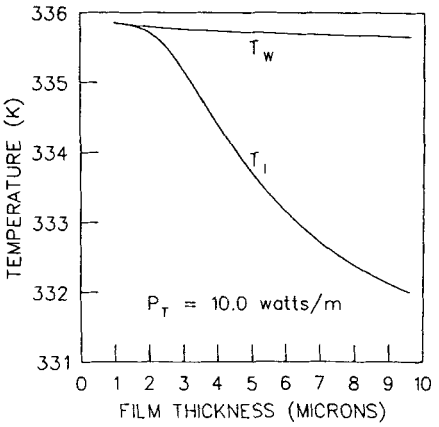


**Figure 12. Predicted wall and interfacial temperature vs. film thickness for $P_T$ = 10.0 W/m.**

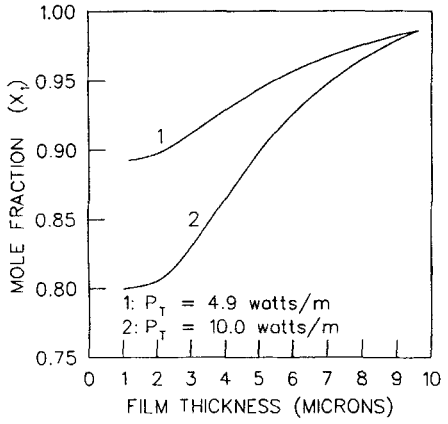


**Figure 13. Predicted mole fraction vs. film thickness for $P_T$ = 4.9 and 10.0 W/m.**

by the film thickness as in Eq. 18. It is easier to discuss the heat flux profile in terms of this equation. As the contact line is approached the thickness decreases, tending to increase the heat flux; but the temperature difference decreases, tending to decrease the heat flux. This is due to the increased temperature at the liquid-vapor interface, which is needed to maintain a constant vapor pressure. Because of these two opposing effects, the evaporative heat flux goes through a maximum that in both cases occurs at a thickness of just greater than 6 $\mu$m and then tends toward zero as the contact line is approached. It is noted that for an extremely pure fluid evaporating into a saturated vapor, the heat flux will increase down to extremely small thicknesses because the interfacial temperature is only a function of the thickness—there are no concentration effects for this case (Neogi and Berryman, 1982).

By Eq. 20 the mass flow rate is related to the heat flux. The local flow rate is presented as a function of film thickness in dimensionless form in Figures 15 and 16. In order to convert the values shown in the figures to flow rates, each term is divided by

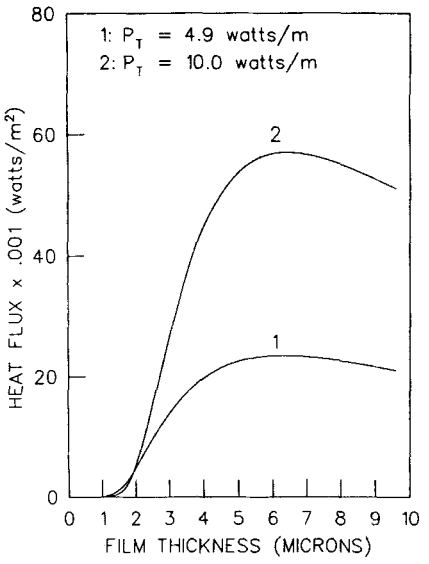


**Figure 14. Predicted heat flux vs. film thickness for $P_T$ = 4.9 and 10.0 W/m.**

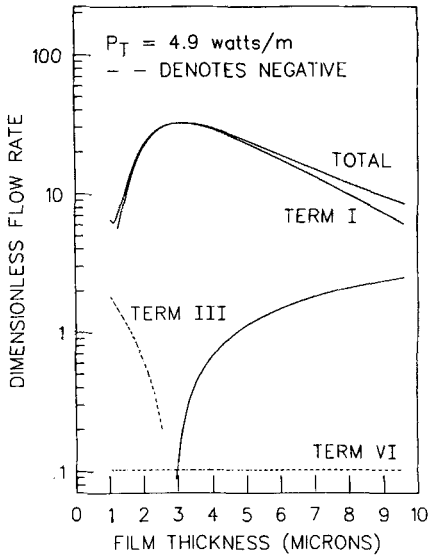


**Figure 15. Dimensionless mass flow rate and individual contributions to dimensionless mass flow rate vs. film thickness for $P_T$ = 4.9 W/m.**

$3\nu/\rho g\delta^3$. We note that since $\delta^3$ varies with position, the large decrease in flow rate with position is not obvious. Using the results obtained for temperature and composition as well as the polynomial fit to the experimental profile data, it is instructive to calculate the contributions to flow as outlined in Eq. 10. Terms II, IV, and V are small over the range of thickness considered. The remaining terms are plotted individually in Figures 15 and 16. Term VI is a constant that depends only on the angle of inclination of the system. Term III depends primarily on the film profile and is thus dependent on the choice of polynomial used to represent the data. It should be noted that this term changes sign as the curvature goes through a maximum, as seen

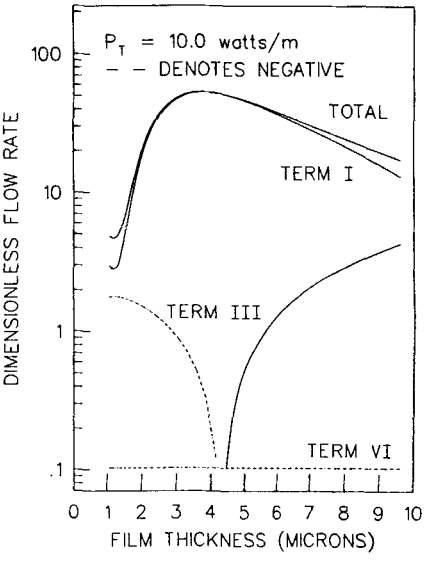


**Figure 16. Dimensionless mass flow rate and individual contributions to dimensionless mass flow rate vs. film thickness for $P_T$ = 10.0 W/m.**

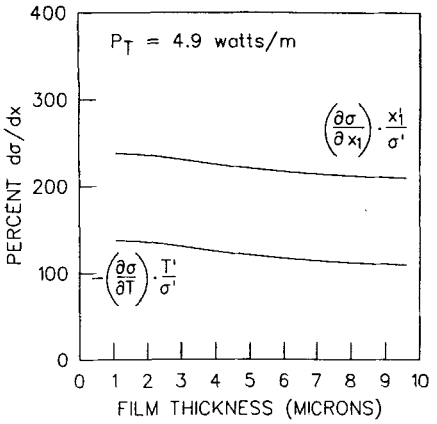


**Figure 17. Percent contributions of temperature gradient and concentration gradient to overall surface tension gradient for $P_T$ = 4.9 W/m.**

in Figures 4 and 6. The major contribution to the flow comes from Term I, which is a result of the surface shear boundary condition given by Eq. 7.

The contribution of the surface shear to the mass flow rate is composed of two parts, as in Equation 12. The percent contributions of temperature gradient and concentration gradient to the total surface tension gradient are plotted in Figures 17 and 18. The sum is, of course, 100%. The single most important mechanism for flow in this evaporating meniscus in the region $10^{-6}$ m $< \delta < 10^{-5}$ m is surface shear caused by a concentration gradient resulting from preferential evaporation of the more volatile component.

Note that only a small portion of two of the many theoretical paths represented in Figure 2 has been analyzed. The concentration at which the shear stress changes sign was not reached, but no doubt the resulting meniscus profile would be very different and possibly unstable beyond this point. Although term I would not induce flow toward the contact line in the region where $\sigma'$ is negative, term IV would do so if the film thickness were sufficiently small. The importance of this term, which was discussed by Wayner et al. (1976) and Wayner and Parks (1985), becomes obvious. Term III is also available as a mechanism for

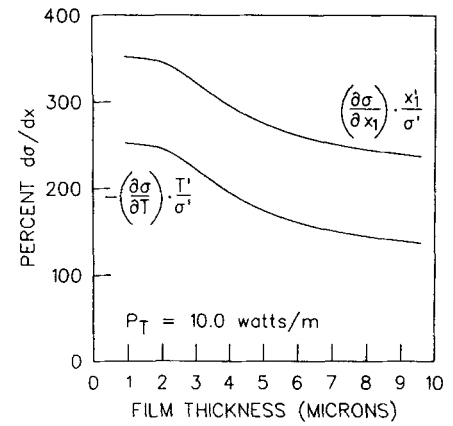


**Figure 18. Percent contributions of temperature gradient and concentration gradient to overall surface tension gradient for $P_T$ = 10.0 W/m.**

flow. The inherent complexity of the flow field in a two-component evaporating meniscus operating under the combined effects of gravity, curvature, and surface shear in the contact line region has been demonstrated. The above analysis gives the relative importance of some of the forces under two of the many possible conditions of flow.

## Acknowledgment

This material is based on work supported by the U.S. Air Force Office of Scientific Research, Air Force System Command, USAF, under Grant No. AFOSR-84-0306, and the U.S. Army Research Office under DAAG29-83-K-0058.

## Notation

$\bar{A}$ = dispersion constant, Eq. 5
$A_{s\ell v}$ = Hamaker constant
$A_i$ = constant for Antoine equation
$a$ = substrate thickness
$a_i$ = constant for surface tension equation
$\bar{B}$ = dispersion constant, Eq. 3
$\bar{B}$ = dispersion constant, Eq. 4
$B_i$ = constant for Antoine equation
$b_i$ = constant for surface tension equation
$C_i$ = constant for Antoine equation
$g$ = acceleration due to gravity
$h_{fg}$ = latent heat of vaporization
$K$ = curvature
$k_\ell$ = thermal conductivity of liquid
$k_s$ = thermal conductivity of substrate
$m$ = order of polynomial
$m_i$ = mass fraction of component $i$
$n$ = constant, Eq. 3
$P = p_\ell + \phi + \rho g x \sin\theta$
$P_{v_i}$ = vapor pressure of component $i$ in solution
$P_{v_i}^{sat}$ = saturation vapor pressure of component $i$
$p_\ell$ = pressure in liquid
$p_v$ = pressure in vapor
$\dot{q}''$ = evaporative heat flux
$T$ = temperature
$T_i$ = interfacial temperature
$u$ = velocity in $x$ direction
$v$ = velocity in $y$ direction
$x$ = direction parallel to substrate
$x_i$ = mole fraction of component $i$
$y$ = direction perpendicular to substrate

### *Greek letters*

$\Gamma$ = mass flow rate
$\delta$ = film thickness
$\theta$ = angle of inclination of plate
$\mu$ = absolute viscosity
$\nu$ = kinematic viscosity
$\rho$ = density
$\sigma$ = surface tension
$\tau_{yx}$ = shear stress in $x$ direction on a surface perpendicular to $y$ direction
$\phi$ = potential energy function
$\phi_B$ = potential of a surface molecule in a bulk phase

### *Literature cited*

Bascom, W. D., R. L. Cottington, and C. R. Singleterry, "Dynamic Surface Phenomena in the Spontaneous Spreading of Oils on Solids," *Contact Angle, Wettability, and Adhesion,* R. F. Gould, ed., *Adv. Chem. Ser.*, Am. Chem. Soc., Washington, DC, **43,** 355 (1964).

Berg, J. C., A. Acrivos, and M. Boudart, "Evaporative Convection," *Advances in Chemical Engineering,* T. B. Drew et al., eds., Academic Press, New York, **6,** 61 (1966).

Chen, J. D., and J. C. Slattery, "Effects of London-van der Waals Forces on the Thinning of a Dimpled Liquid Film as a Small Drop or

Bubble Approaches a Horizontal Solid Plane," *AIChE J.*, **28,** 955 (1982).
Churaev, N. V., "Molecular Forces in Wetting Films of Nonpolar Liquids. 1: Thick Films," *Colloid J. USSR (Engl. trans.)*, **36,** 318 (1974a).
———, "Molecular Forces in Wetting Films of Nonpolar Liquids. 2: Thin Films," *Colloid J. USSR (Engl. trans.)*, **36,** 323 (1974b).
———, "Calculation of Dispersion Forces in the Transitional Region of Interbody Distances," *Colloid J. USSR (Engl. trans.)*, **37,** 730 (1975).
Cook, R., C. Y. Tung, and P. C. Wayner, Jr., "Use of Scanning Microphotometer to Determine the Evaporative Heat Transfer Characteristics of the Contact Line Region," *J. Heat Transfer*, **103,** 325 (1981).
Deryagin, B. V., S. V. Nerpin, and N. V. Churaev, "Effect of Film Transfer upon Evaporation of Liquids from Capillaries," *RILEM Bull.*, **29,** 93 (1965).
Dzyaloshinskii, I. E., E. M. Lifshitz, and L. P. Pitaevskii, "The General Theory of Van der Waals Forces," *Adv. Phys.*, **10,** 165 (1961).
Edwards, D. K., A. Balakrishnan, and I. Catton, "Power-Law Solutions for Evaporation from a Finned Surface," *J. Heat Transfer*, **96,** 423 (1974).
Frenkel, J., *Kinetic Theory of Liquids*, Dover, New York (1955).
Gear, C. W., *Numerical Initial Value Problems in Ordinary Differential Equations*, Prentice-Hall, Englewood Cliffs, NJ (1971).
Hindmarsh, A. C., "GEAR: Ordinary Differential Equation Solver," Lawrence Livermore Lab. Rep. UCID-30001, Revision 3 (1974).
Holm, F. W., and S. P. Goplen, "Heat Transfer in the Meniscus Thin-Film Transition Region," *J. Heat Transfer*, **101,** 543 (1979).
Huh, C., and L. E. Scriven, "Hydrodynamic Model of Steady Movement of a Solid/Liquid/Fluid Contact Line," *J. Colloid Interf. Sci.*, **35,** 85 (1971).
Jasper, J. J., "The Surface Tension of Pure Liquid Compounds," *J. Phys. Chem. Ref. Data*, **1,** 841 (1972).
Kenning, D. B. R., "Two-Phase Flow With Nonuniform Surface Tension," *Appl. Mech. Rev.*, **21,** 1101 (1968).
Ludviksson, V., and E. N. Lightfoot, "The Dynamics of Thin Liquid Films in the Presence of Surface-Tension Gradients," *AIChE J.*, **17,** 1166 (1971).
Miller, C. A., and E. Ruckenstein, "The Origin of Flow during Wetting of Solids," *J. Colloid Interf. Sci.*, **48,** 368 (1974).
Mirzamoghadam, A. V., and I. Catton, "Holographic Interferometry Investigation of Meniscus Behavior," *Multiphase Flow and Heat Transfer, HTD*, V. K. Dhir et al., eds., ASME, New York, **47,** 49 (1985a).
———, "A Physical Model of the Evaporating Meniscus, *Augmentation of Heat Transfer in Energy Systems, HTD*, P. J. Bishop, ed., ASME, New York, **52,** 47 (1985b).
Moosman, S., and G. M. Homsy, "Evaporating Menisci of Wetting Fluids," *J. Colloid Interf. Sci.*, **73,** 212 (1980).
Neogi, P., and J. B. Berryman, "Stability of Thin Liquid Films Evaporating into Saturated Vapor," *J. Colloid Interf. Sci.*, **88,** 100 (1982).
Parks, C. J., and P. C. Wayner, Jr., "Fluid Flow in an Evaporating Meniscus of a Binary Mixture in the Contact Line Region: Constant Vapor Pressure Boundary Condition," AIChE Ann. Meet., Chicago (1985).
Potash, M., Jr., and P. C. Wayner, Jr., "Evaporation from a Two-Dimensional Extended Meniscus," *Int. J. Heat Mass Transfer*, **15,** 1851 (1972).
Reid, R. C., J. M. Prausnitz, and T. K. Sherwood, *The Properties of Gases and Liquids*, 3rd Ed., McGraw-Hill, New York (1977).
Renk, F. J., and P. C. Wayner, Jr., "An Evaporating Ethanol Meniscus. I: Experimental Studies," *J. Heat Transfer*, **101,** 55 (1979).
Renk, F., P. C. Wayner, Jr., and G. M. Homsy, "On the Transition between a Wetting Film and a Capillary Meniscus," *J. Colloid Interf. Sci.*, **67,** 408 (1978).
Ruckenstein, E., and R. K. Jain, "Spontaneous Rupture of Thin Liquid Films," *J. Chem. Soc. Faraday Trans. II*, **70,** 132 (1974).
Sharp, R. R., "The Nature of Liquid Film Evaporation During Nucleate Boiling," NASA Rep. TN D-1999 (1964).
Scriven, L. E., and C. V. Sternling, "The Marangoni Effects," *Nature*, **187,** 186 (1960).
Tung, C. Y., "Evaporative Heat Transfer in the Contact Line of a Mixture," Ph.D. Thesis, Rensselaer Polytech. Inst., Troy, NY (1982).
Tung, C. Y., T. Muralidhar, and P. C. Wayner, Jr., "Experimental Study of Evaporation in the Contact Line Region of a Mixture of Decane and 2% Tetradecane," *Proc. 7th Int. Heat Transfer Conf.*, **4,** 101 (1982).
Tung, C. Y., and P. C. Wayner, Jr., "Effect of Surface Shear on Fluid Flow in an Evaporating Meniscus of a Mixture of Alkanes," *Proc. 5th Int. Heat Pipe Conf.* JATEC, Tokyo, Pt. 1, 201 (1984).
Voutsinos, C. M., and R. L. Judd, "Laser Interferometric Investigations of the Microlayer Evaporation Phenomena," *J. Heat Transfer*, **97,** 88 (1975).
Wayner, P. C., Jr., "The Effect of London-van der Waals Dispersion Force on Interline Heat Transfer," *J. Heat Transfer*, **100,** 155 (1978).
———, "Interfacial Profile in the Contact Line Region of a Finite Contact Angle System," *J. Colloid Interf. Sci.*, **77,** 495 (1980).
Wayner, P. C., Jr., Y. K. Kao, and L. V. LaCroix, "The Interline Heat Transfer Coefficient of an Evaporating Wetting Film," *Int. J. Heat Mass Transfer*, **19,** 487 (1976).
Wayner, P. C., Jr., and C. J. Parks, "Effect of Liquid Composition on Enhanced Flow Due to Surface Shear in the Contact Line Region: Constant Vapor Pressure Boundary Condition," *Multiphase Flow and Heat Transfer, HTD*, V. K. Dhir et al., eds., ASME, New York, **47,** 57 (1985).
Wayner, P. C., Jr., M. Tirumala, S. C. Y. Tung, and J. H. Yang, "Fluid Flow in the Contact Line Region of a Mixture of Alkanes: 98% Hexane and 2% Octane," AIAA 18th Thermophys. Conf., Montreal (1983).
Wayner, P. C., Jr., C. Y. Tung, M. Tirumala, and J. H. Yang, "Experimental Study of Evaporation in the Contact Line Region of a Thin Film of Hexane," *J. Heat Transfer*, **107,** 182 (1985).

*Manuscript received Mar. 10, 1986, and revision received July 15, 1986.*